Plasmodium falciparum disruption of pericyte angiopoietin-1 secretion contributes to barrier breakdown in a 3D brain microvessel model

Rory K. M. Long[1,2], François Korbmacher[1], Paolo Ronchi[3], Hannah Fleckenstein[1,3], Waleed Mirza[1], Mireia Mallorquí[1], Ruth Aguilar[4], Gemma Moncunill[4], Yannick Schwab[3], Maria Bernabeu[1*]

[1]*European Molecular Biology Laboratory (EMBL) Barcelona, Barcelona, Spain*
[2]*Heidelberg University, Faculty of Biosciences, Heidelberg, Germany*
[3]*European Molecular Biology Laboratory (EMBL), Cell Biology and Biophysics Unit, Heidelberg, Germany.*
[4]*Barcelona Institute for Global Health (ISGlobal), Hospital Clínic-Universitat de Barcelona, Barcelona, Spain*

*To whom correspondence should be addressed. Email: maria.bernabeu@embl.es

Abstract:

Disruption of the angiopoietin-Tie axis is a common finding in cerebral malaria (CM) patients. Increased concentrations of angiopoietin-2 (Ang-2) and decreased levels of angiopoietin-1 (Ang-1) correlate with disease severity and have been proposed as biomarkers of CM. Brain pericytes have a key role in promoting vascular quiescence through many pathways, including Ang-1 secretion. Despite evidence of pericyte damage on post-mortem samples of CM patients, their role in the pathogenesis of the disease remains unexplored. To address this question, we engineered a 3D microfluidics-based cerebral microvessel model containing both human primary cerebral microvascular endothelial cells and cerebral vascular pericytes. This model replicated pericyte vessel coverage and ultrastructural endothelial-pericyte interactions present in the *in vivo* brain microvascular bed. 3D brain microvessels experienced an increase in vascular permeability after exposure to purified *P. falciparum*-iRBC egress products. This was accompanied by minor changes in pericyte ultrastructural morphology detected by serial block-face scanning electron microscopy. Luminex quantification of cytokines secreted by bioengineered microvessels revealed a significant decrease in Ang-1 secretion and increase in the Ang-2/Ang-1 ratio, suggesting that *P. falciparum*-iRBC egress products directly disrupt pericyte biology. Furthermore, we show that pre-incubation with recombinant Ang-1 partially protects against microvessel barrier breakdown caused by *P. falciparum*-iRBC egress products. Our approach

highlights a novel role of brain pericytes in CM pathogenesis and indicates that dysregulation in the angiopoietin-Tie axis contributes to *P. falciparum*-mediated vascular dysfunction.

Significance:

Cerebral malaria is caused by brain endothelial disruption mediated by *Plasmodium falciparum* infection. However, the contribution of other brain vascular cell types in disease pathogenesis remains unexplored. Here, we created an *in vitro* model of the brain microvasculature comprised of brain endothelial cells and pericytes, a cell type that supports vascular quiescence. We found that barrier disruptive products released from *Plasmodium falciparum*-infected red blood cells trigger minor pericyte morphological changes and inhibit the secretion of angiopoietin-1, a key barrier protective endothelial ligand. The external addition of angiopoietin-1 into the model partially restored microvascular barrier function after exposure to *P. falciparum* egress products, highlighting the role of brain pericytes in cerebral malaria formation and suggesting future therapeutic avenues.

Introduction:

Cerebral malaria (CM) is a severe neurological complication of *Plasmodium falciparum* infection, clinically characterized by coma and fatality rates averaging 15-20% (1). Furthermore, approximately 20% of CM survivors endure lifelong neurological sequelae such as hemiplegia, ataxia, epilepsy or speech disorders (2). The majority of pediatric CM-related deaths present severe brain swelling due to vasogenic edema, likely as a consequence of blood-brain barrier dysfunction (3). A hallmark of CM is the sequestration of *P. falciparum*-infected red blood cells (iRBC) in the brain microvasculature (4). While the molecular players responsible for *P. falciparum*-iRBC ligand-receptor interactions with cerebral endothelial cells have been extensively studied (5–7), the consequences of iRBC sequestration to the brain microvasculature require further investigation. Nevertheless, evidence suggests that the increase in vascular permeability is a result of a multifaceted process including a blockade of barrier-supportive endothelial receptors by iRBC, the release of toxic *P. falciparum* products from egressed iRBC, and a dysregulated host innate immune response (8, 9).

An important pathway commonly dysregulated in CM patients is the angiopoietin-Tie axis, crucial to maintaining endothelial pro-barrier, anti-inflammatory, and anti-apoptotic functions (10). Binding of the vascular ligand angiopoietin-1 (Ang-1) to the endothelial receptor Tie-2 promotes vascular quiescence and the stabilization of endothelial tight junction proteins, such as Occludin

and Zona Occludens-1 (ZO-1), necessary for maintaining the barrier function of the brain microvasculature (11–13). Conversely, angiopoietin-2 (Ang-2), which is rapidly released from small endothelial storage granules called Weibel-Palade bodies, generally acts as a Tie-2 antagonist leading to endothelial activation and vascular leakage (14). Given the opposing roles of these two molecules in vascular function, increased levels of Ang-2 and decreased levels of Ang-1 have been largely associated with cerebral vascular pathogenesis in a multitude of diseases (15, 16). Similarly, a decrease in Ang-1, an increase in Ang-2 and the serum Ang-2:Ang-1 ratio has been well documented in fatal cases of both pediatric and adult CM (17–21). Despite its importance, the mechanisms leading to angiopoietin-Tie axis disruption in CM are poorly understood. Human pro-inflammatory cytokines and pro-coagulation proteins, such as TNF-α and thrombin, have been proposed as responsible for the increase of Ang-2 secretion by endothelial cells (22, 23), but the causative agent responsible for decreased secretion of Ang-1 in CM patients remains unknown.

Smooth muscle cells and pericytes are the main cellular sources for Ang-1 secretion in the brain microvasculature (10). Beyond Ang-1 secretion, pericytes support the microvasculature and promote quiescence through additional roles. Structurally, pericytes wrap around cerebral microvessels and interact with the endothelium through reciprocal ultrastructural membrane protrusions, known as peg-and-socket junctions (24), and secrete extracellular matrix components of the microvascular basal lamina that strengthen microvascular architecture. Functionally, pericytes regulate brain blood flow by controlling vessel diameter through constriction (25). Cerebral pericytes have been implicated in various vascular disorders of the central nervous system. Loss of pericytes from the cerebral vasculature in ischemic stroke and Alzheimer's disease is associated with blood-brain barrier disruption, extravasation of blood components into the brain parenchyma, and neuronal loss (26–28). Similarly, histopathological studies in retinal samples of fatal pediatric CM cases have revealed pericyte damage in regions of *P. falciparum*-iRBC sequestration, suggesting a similar role of these cell types in severe malaria infections (29). Yet, the role of cerebral pericytes in CM pathogenesis and in the dysregulation of the angiopoietin-Tie pathway remains largely unknown.

Bioengineered vascular models are emerging as powerful tools to study disease mechanisms *in vitro.* They have been successfully used to recapitulate many aspects of *in vivo* vascular disease including dysfunction of the angiopoietin-Tie pathway (30), and more recently, malaria pathogenesis, by modeling ligand-receptor interaction of *P. falciparum*-iRBC in microvessels (31) or transcriptional changes on endothelial cells upon exposure to *P. falciparum*-iRBC (32). Here,

we have further developed our existent 3D brain microvascular model (31), with the addition of pericytes to create a device that recapitulates *in vivo* interactions between both cell types. We have used this advanced model to understand the molecular basis of angiopoietin-Tie dysregulation in CM. Our results indicate that *P. falciparum*-iRBC and products released during parasite blood stage egress play a role in angiopoietin-Tie dysregulation, and propose brain pericytes as a new player in CM pathogenesis.

Results:

In vitro 3D brain microvessel model recapitulates *in vivo* cerebral endothelial-pericyte interactions

To investigate the role of cerebral pericytes in *P. falciparum*-mediated vascular pathogenesis, we have generated a 3D brain microvessel model that recapitulates the degree of pericyte coverage of the endothelium present in the brain microvasculature. The device is fabricated in a collagen type I hydrogel containing a microfluidic network with a pre-defined geometry, which is connected to both an inlet and outlet, enabling vessel perfusion (33). Previous incorporation of pericytes in similar bioengineered 3D models involved cellular addition into the collagen hydrogel itself, however, this resulted in sparse interaction of pericytes with the endothelial microvessels (33). Indeed, cerebral pericytes have been shown to cover approximately one third of the brain microvasculature, albeit with slight variations along the brain vascular hierarchical network (34, 35). In this model, primary human brain vascular pericytes (HBVP) were seeded directly into the channels along with primary human brain microvascular endothelial cells (HBMEC) at a 5:1 endothelial to pericyte ratio (Fig. 1*A*). After 3 days in culture, the two cell types appear to reorganize into two different layers with luminal endothelial cells and mCherry-expressing pericytes wrapping around the endothelial cells (Fig. 1*B*). Pericytes distributed homogenously around the vessel cross-section, with approximately a third of the microvessel surface area covered by pericytes (29.6% of the bottom surface and 27.3% of the top surface) (Fig. 1*C*). Notably, endothelial VE-cadherin junctional labeling is continuous along the vessel luminal surface, suggesting that pericyte presence does not disrupt the endothelial layer (Fig. 1*D*). Furthermore, endothelial cells in the microvessel network express other common cerebral endothelial adherens and tight junction markers, such as β-catenin and ZO-1 respectively (Fig. 1*E*). Labeling by α-smooth muscle actin (αSMA) shows that pericytes appear as elongated cells with thin processes stretching over multiple endothelial cells located abluminally between the

endothelial layer and the collagen hydrogel, as suggested by an orthogonal view (Fig. 1*D*). Pericyte cellular identity was confirmed by the expression of a combination of cerebral pericyte cellular markers including αSMA (Fig. 1*D*), platelet derived growth factor receptor β (PDGFRβ) and nerve/glial antigen 2 (NG-2) (Fig. 1*E*) (36, 37). Importantly, labeling of cerebral pericytes colocalized with laminin and collagen IV staining, suggesting that pericytes contribute to the secretion of extracellular matrix components that compose the basal lamina *in vivo* (Fig. 1*E*) (38).

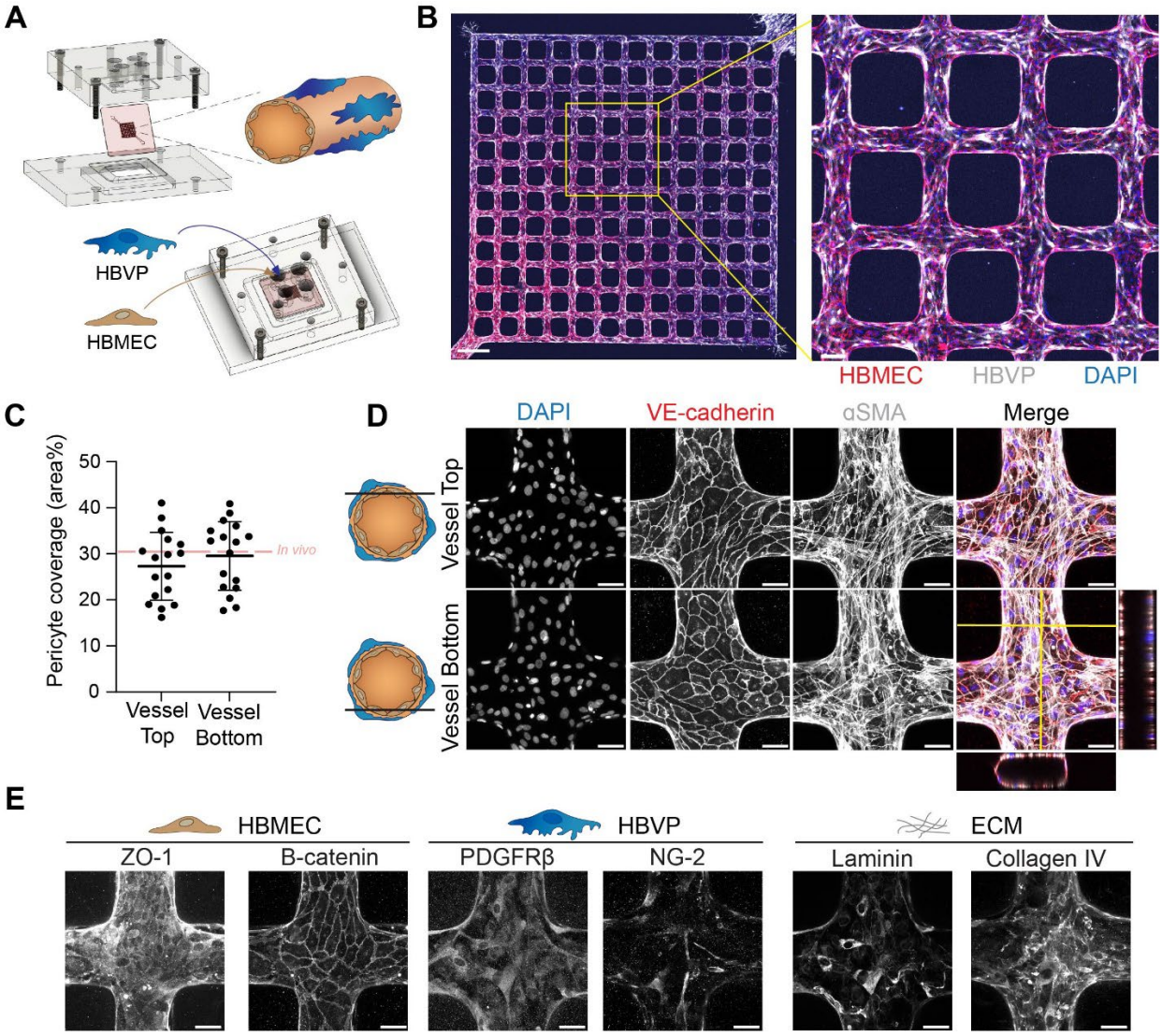

Fig. 1. A microfluidics-based 3D brain microvessel model recapitulates *in vivo* brain vascular architecture and pericyte coverage. *(A)* Schematic depiction of the fabrication pieces and device set-up (top-left), including a representation of resultant endothelial-pericyte interactions (top-right). Schematic depiction of the seeding method used to generate the 3D microvessel model

(bottom). *(B)* Immunofluorescence assay (IFA) maximum z-projection of the full network of cellularized channels labeled with Von-Willebrand factor for HBMEC (red), mCherry expressing HBVP (white) and DAPI (blue) (left). Inset highlighting pericyte coverage of the microvessels (right). Scale bars represent 500 μm and 100 μm (Inset) *(C)* Quantification of the percentage of endothelial microvessel area covered by pericytes on either the top or bottom microvessel surface in a z cross-sectional view. Red dashed line represents estimated *in vivo* brain microvascular pericyte coverage. Data points represent quantification of 17 devices with statistical analysis determined by Mann-Whitney U test. Error bars represent mean +/- standard deviation. *(D)* IFA maximum z-projection of VE-cadherin, αSMA, and DAPI labeling on the top and bottom cross-sectional surfaces of microvessels (left). Merge and orthogonal view with VE-cadherin (red), αSMA (white) and DAPI (blue) (right). *(E)* IFA maximum z-projection of brain endothelial markers, ZO-1 and β-catenin, brain pericyte markers, NG-2 and PDGFRβ, and extracellular matrix markers, laminin and collagen IV. Scale bars represent 50 μm in D and E.

Volumetric electron microscopy has been previously used to characterize *in vivo* 3D ultrastructural interactions between pericytes and endothelial cells of the cerebral microvasculature (24). To characterize the spatial and ultrastructural organization of pericytes and endothelial cells in the model, we utilized Serial Block-Face Scanning Electron Microscopy (SBF-SEM) (39), a volume electron microscopy technique that provides nanometer resolution of samples in a large field of view (40). We imaged a 100 μm segment of a microvessel branch with a 15x15x50 nm xyz resolution, followed by cellular segmentation and rendering. We characterized microvessel coverage of approximately 25 individual pericytes, distinguished from endothelial cells by the presence of a highly granulated cytoplasm (41). Cross-sectional analysis and segmentation of the microvessel revealed an ovoid microvessel morphology, and confirmed the presence of pericytes at the abluminal side of the endothelial cells (Fig. 2*A*). Pericytes acquired a classical bump-on-a-log morphology, with the soma being the thickest region of the cell, and their longitudinal axis aligned with the direction of flow (Fig. 2*B*). Most of the endothelial-pericyte interface is composed of thin pericytic lamellae (100-300 nm thickness) that cover large areas of the endothelial surface, with multiple thin pericytic branches appearing mostly at the cell periphery, as described previously (24). A close up of regions of pericyte-endothelial cell interaction reveal that the membranes of both cell types are in close proximity, even though peg-and-socket junctions were not found (Fig. 2*C*). Although pericytes constitute a heterogenous cell population depending on their location within the vascular branch, their morphology in the model, coverage of endothelial cells, and co-staining of αSMA, PDGFRβ and NG-2 (Fig. 1*D-E*) are reminiscent of ensheathing pericytes commonly found in arterioles (42, 43). Overall, the 3D *in vitro* brain microvessel model recapitulates *in vivo* interactions between cerebral endothelial cells

and pericytes, both at the tissue and ultrastructural level, that can next be utilized to model the role of pericytes in malaria pathogenesis.

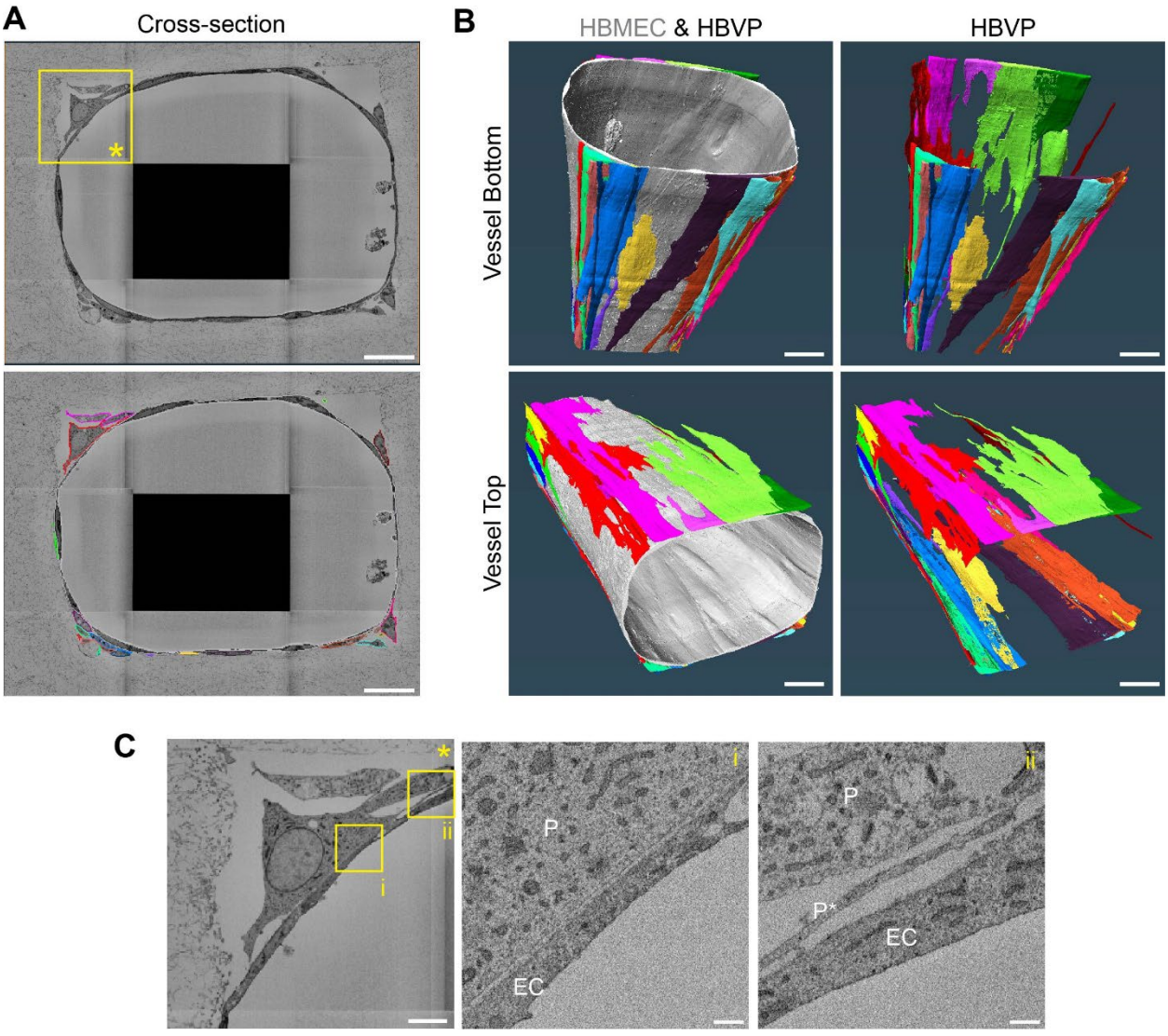

Fig. 2. Serial Block-Face Scanning Electron Microscopy reveals ultrastructural interactions between pericytes and endothelial cells. *(A)* A cross-section of the microvessel imaged through the SBF-SEM volume (top) and the corresponding segmentation outlines of the endothelium (grey) and surrounding pericytes (coloured). Scale bars represent 20 µm. *(B)* 3D rendering of the segmented microvessel (grey) and the surrounding pericytes viewed from below and above. Scale bars represent 10 µm. *(C)* Zoomed images of the ROI in A. Insets show ROIs i and ii where pericytes are denoted with "P", endothelial cells by "EC" and pericyte lamellae by "P*". Scale bars represent 5 µm (left) and 500 nm in the insets (center and right).

P. falciparum egress products increase vessel permeability but only cause minor changes in pericyte morphology

Multiple *in vitro* studies have shown that *P. falciparum* products released during malaria parasite egress disrupt the endothelial barrier (44–48). To characterize the impact that these could have on pericyte function, we established a protocol to create media enriched for *P. falciparum*-iRBC egressed products, denoted from here on as iRBC-egress media. Briefly, tightly synchronized schizont stage-iRBCs were purified and allowed to egress in vascular growth media, followed by recovery of the supernatant fraction containing *P. falciparum* soluble products at an estimated concentration of $5x10^7$ruptured iRBC/mL (equivalent to simultaneous egress of approximately a 1% parasitemia) (Fig. S1*A*-*B*). We measured the endothelial disruptive properties of iRBC-egress media by the xCELLigence system, which provides real time measurement of cell barrier integrity through impedance. The *P. falciparum* egress products caused a significant, dose-dependent decrease in cell index, a measurement of monolayer barrier function normalized to untreated cells, that reached a maximum disruption at 18 hours (Fig. S1*C*). To elucidate if iRBC-egress media also induces barrier breakdown in the brain 3D microvessel model, we performed permeability assays in a simpler microvessel network which consists of a single 200 μm channel. After perfusion and incubation with iRBC-egress media for 18 hours, *P. falciparum* egress products accumulated on the lateral and bottom walls of the microvessel and appeared as dark spots in brightfield that were DAPI-positive by confocal microscopy, suggesting the presence of hemozoin, food vacuoles and parasite DNA remnants (Fig. 3*A* and *B*). Channels perfused with iRBC-egress media presented a significant increase to 70 kDa FITC-dextran permeability across the entire vessel wall, corresponding to a 6-fold increment compared to vessels perfused with vascular cell media (Fig. 3*B* and *C*).

To determine whether increased permeability was associated with physical changes in pericytes, we assessed their cellular morphology in 3D microvessels exposed to iRBC-egress media for 18-hours by SBF-SEM. Pericytes maintained close spatial proximity to the endothelium in the presence of *P. falciparum*-iRBC ghosts, similar to control devices exposed to vascular growth media (Fig. 3*D*). To investigate potential changes in pericyte shape, we isolated and analyzed each 3D rendered pericyte (Fig 3*E-F; S2*). Cellular features such as circularity and maximum width did not differ between conditions, however, iRBC-egress media treated pericytes presented fewer branches suggesting a response to iRBC-egress media (Fig. 3*E-F*). Altogether, our results

show that *P. falciparum* egress products cause an increase in permeability of the 3D brain microvessel model, accompanied by minor changes in pericyte morphology.

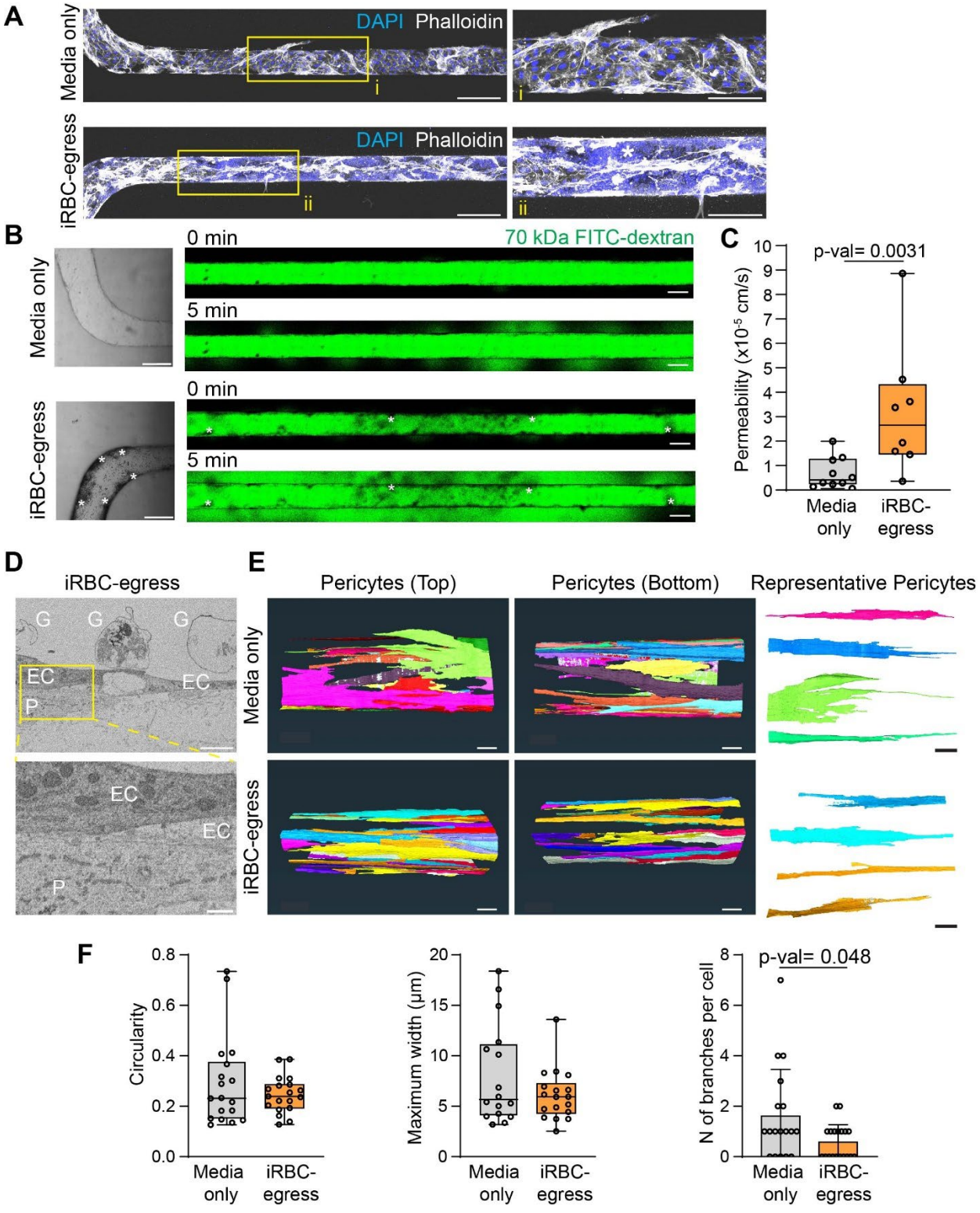

Fig. 3. iRBC-egress media increases vessel permeability and induces minor morphological changes in pericytes. *(A)* Fluorescence confocal imaging of phalloidin (white) and DAPI (blue) of single channel 3D brain microvessels treated with either media-only or *P. falciparum*-iRBC-egress media for 18-hours. Insets show ROIs of i and ii that highlight endothelial junctions and pericyte coverage (phalloidin). Accumulated DAPI-positive *P. falciparum*-iRBC egress material is denoted by an asterisk. Scale bars represent 200 μm (left) and 50 μm in inset (right). *(B)* Brightfield images near the inlet of 3D brain microvessels after 18-hour incubation with media-only or iRBC-egress media (left). Representative confocal images of 70 kDa FITC-dextran flux into the surrounding collagen 0 and 5 minutes after perfusion (right). Accumulated *P. falciparum*-iRBC egress material is represented with asterisks. Scale bars represents 200 μm. *(C)* Apparent permeability of 70 kDa FITC-dextran in channels treated with media only or *P. falciparum*-iRBC egress media for 18-hours. Data points represent 8 individual devices. *(D)* SBF-SEM image and zoomed ROI of microvessels treated with iRBC-egress media. Pericytes are denoted as "P", endothelial cells by "EC" and iRBC ghosts by "G". Scale bar represents 2 μm (top) and 500 nm in inset (bottom). *(E)* 3D rendering of pericytes segmented from microvessels treated with media-only or iRBC-egress media and imaged with SBF-SEM (left). Representative segmented pericytes for morphology analysis (right). Scale bar represents 10 μm. *(F)* Circularity, maximum width and number (N) of branches analysis of 16-18 segmented pericytes. Box and whisker plots display the median, 25th and 75th percentiles and the minimum and maximum data points, and statistical significance was measured by Mann-Whitney U test in both C and F.

P. falciparum-iRBCs induce dysregulation of the angiopoietin-Tie axis

To determine whether parasite egress products are a major driver of angiopoietin-Tie axis disruption characteristic of CM (17–20, 49), we used a Luminex assay to measure secreted protein concentrations in microvessel supernatants recovered after 18-hour incubation with iRBC-egress media. Remarkably, we observed a substantial decline of Ang-1 secretion by pericytes, with concentrations nearly reaching the baseline level detected in acellular vascular growth media (Fig. 4*A*). Consistent with recent studies on 2D HBMEC monolayers (22), iRBC-egress media incubation did not result in increased Ang-2 secretion. Indeed, we quantified a significant decrease in Ang-2 secretion (Fig. 4*A*). Despite Ang-2 decrease, a significant increase in the Ang-2/Ang-1 ratio was found, after Ang-1 and Ang-2 concentrations were subtracted against concentrations found in the acellular vascular growth media (Fig. 4*A*). Additionally, we observed a decrease in 3D microvessel secretion or shedding of other vascular factors important for endothelial-pericyte interaction, such as Neural cadherin (N-cadherin) and Tissue Inhibitor of Metalloproteinase-1 (TIMP-1) (Fig. S3*A*). Conversely, we detected no changes in Vascular Endothelial Growth Factor (VEGF), Tie-2, Angiopoietin-like-4 (ANGPTL4), Platelet Derived Growth Factor-BB (PDGF-BB), Interleukin-8 (IL-8) or Chemokine Ligand-1 (CXCL-1) after 18-hour incubation with iRBC-egress media (Fig S3).

To validate whether changes in the angiopoietin-Tie axis occur physiologically following *P. falciparum* blood stage egress within the microvasculature, we perfused the 3D brain microvessels with schizont stage *P. falciparum*-iRBC for 30 minutes followed by a 10-minute wash. After an 18-hour incubation period, supernatants were again recovered and analyzed by Luminex. Similar results were obtained, with a reduction in both Ang-1 and Ang-2 secretion and an increase in the Ang-2/Ang-1 ratio (Fig. 4*B*). Altogether, these results suggest that *P. falciparum*-iRBC hamper Ang-1 secretion by pericytes, revealing a previously unappreciated role of pericytes in the dysregulation of the angiopoietin-Tie axis in cerebral malaria.

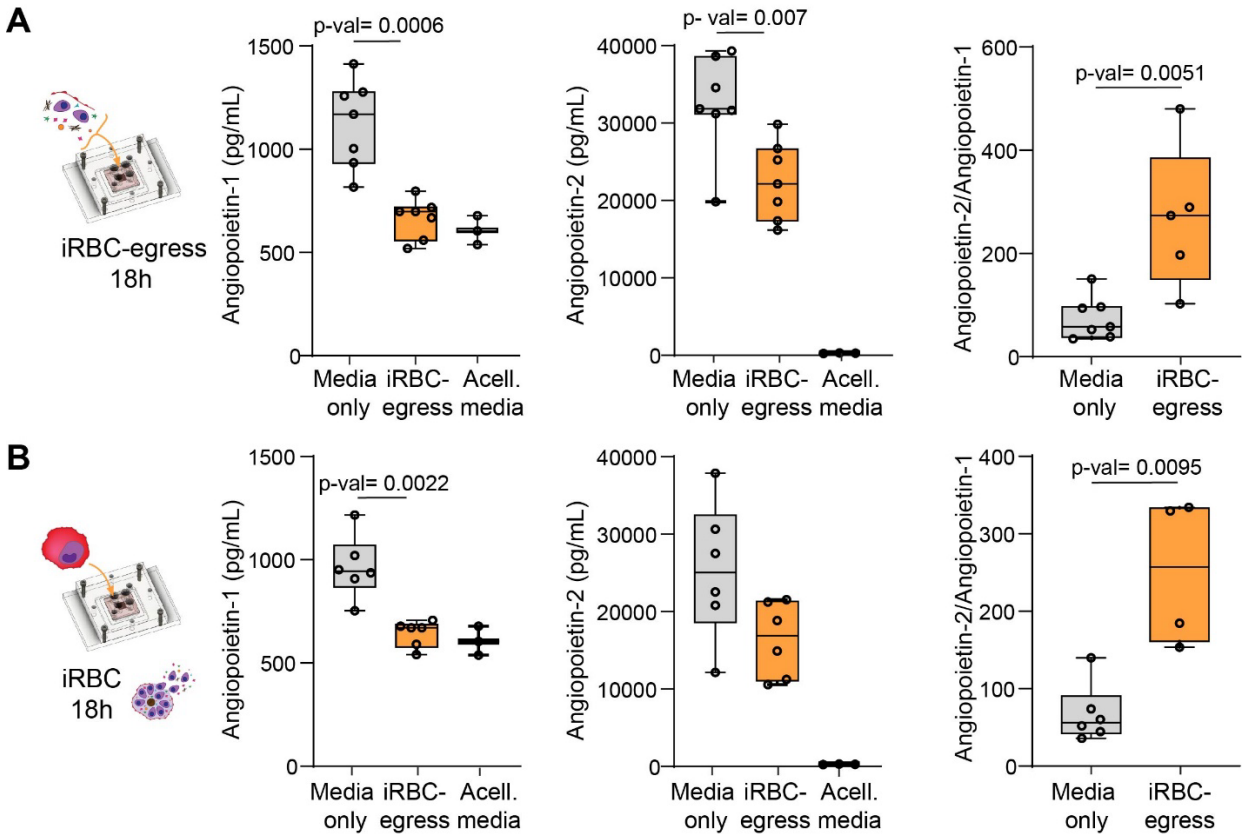

Fig. 4. *P. falciparum*-iRBC-egress media and intact *P. falciparum*-iRBC induce angiopoietin-Tie axis dysregulation. *(A)* Ang-1 and Ang-2 concentrations measured from 3D brain microvessels treated with media-only, iRBC-egress media for 18-hours or from acellular media before culture (Acell. Media) (left and center). Ang-2: Ang-1 ratio in supernatants collected from 3D brain microvessels normalized to corresponding acellular media protein concentrations (right). *(B)* Ang-1 and Ang-2 concentrations measured from 3D brain microvessels treated with media-only, *P. falciparum*-iRBC for 18-hours or from acellular media before culture (Acell. Media) (left and center). Ang-2: Ang-1 ratio in supernatants collected from 3D brain microvessels normalized to corresponding acellular media protein concentrations (right). Box and whisker plots display the median, 25th and 75th percentiles and the minimum and maximum data points in A and B. Data points represent supernatants pooled from 2-3 devices in 6-7 independent experiments and were

analyzed by Mann-Whitney U test. Acellular media measures were obtained from 3 independent aliquots. Data points in which Ang-1 concentrations measured from 3D brain microvessels were below the concentrations in acellular media were removed to calculate the Ang-2: Ang-1 ratio.

Recombinant Ang-1 partially protects against endothelial barrier breakdown by iRBC-egress media

Given the key role of Ang-1 to promote vascular quiescence and endothelial barrier formation we investigated whether Ang-1 supplementation could protect against the barrier disruptive effects of iRBC-egress media. First, we measured barrier disruption by xCELLigence in a 2D *in vitro* endothelial culture in the absence of pericytes. Furthermore, the 18-hour pre-treatment of rAng-1 to resting endothelium caused a non-significant minor decrease in endothelial permeability. Conversely, an 18-hour pre-treatment of recombinant Ang-1 (rAng-1), prior to the incubation with iRBC-egress media and rAng-1, partially protected against endothelial barrier disruption (Fig. 5*A-C*). While both iRBC-egress media conditions follow parallel endothelial breakdown trajectories, rAng-1 addition dampened the maximum levels of disruption by iRBC-egress media, and was followed by a faster recovery to endothelial monolayer baseline levels (Fig. 5*B*). Indeed, pre-treatment with rAng-1 conferred a 35% barrier breakdown protection after normalization to the untreated endothelial condition (Fig. 5*C*). Nevertheless, shorter pre-treatment periods with rAng-1 (1-hour) did not protect against iRBC-egress media disruption, suggesting that the establishment of endothelial protective pathways is not immediate (Fig. S4).

Next, we tested the protective capacity of rAng-1 against iRBC-egress products in the 3D microvessel model (Fig. 5*D*). While 3D microvessel permeability values to 70 kDa FITC-dextran presented a 6.5-fold increase upon exposure to iRBC-egress media, permeability values only increased by 1.5-fold following an iRBC-egress media challenge after an 18-hour pre-treatment with rAng1 (Fig. 5*E-G*). Overall, rAng-1 conferred statistically significant protection to the barrier breakdown properties exerted by iRBC-egress media (Fig. 5*G*). Taken together, pre-treatment with rAng-1 partially protects against microvascular permeability caused by *P. falciparum* egress products, both in 2D and 3D, highlighting the importance that a decrease in Ang-1 could have in CM pathogenesis.

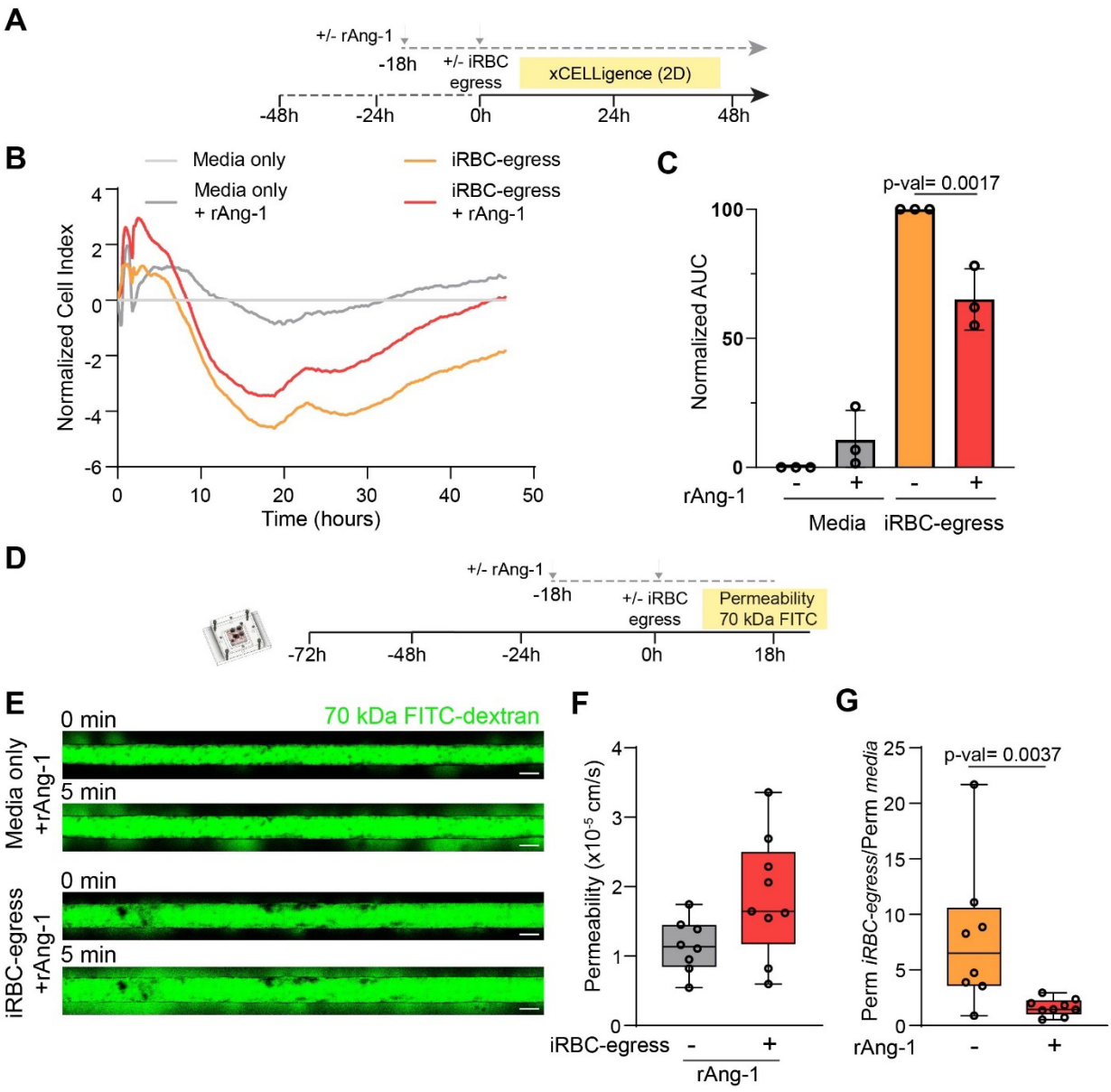

Fig. 5. Recombinant Ang-1 (rAng-1) partially protects against increased permeability induced by iRBC-egress media. *(A)* Experimental outline of the rAng-1 pre-treatment permeability experiment measured in 2D HBMEC monolayers in the absence of HBVP. *(B)* Representative recording data of xCELLigence measurements taken after an 18-hour +/- rAng-1 pre-treatment followed by +/- iRBC-egress media addition. All conditions were normalized to the media only control. *(C)* Area under the curve analysis of 3 independent experiments run in triplicate with iRBC-egress media normalized as 100. Error bars are mean +/- standard deviation. Statistical significance is measured by repeated measures one-way ANOVA test with Dunnett's multiple comparisons test. *(D)* Experimental outline of the rAng-1 pre-treatment permeability experiment on 3D brain microvessels. *(E)* Confocal image of the 70 kDa FITC-dextran flux into the surrounding collagen at 0 and 5 minutes after dextran perfusion. Images correspond to a representative rAng-1 pretreated microvessel exposed to either media-only or iRBC egress media for 18 hours. Scale bars represent 200 μm. *(F)* Apparent permeability of 70 kDa FITC-dextran in channels pretreated

with rAng-1 followed by 18-hour media-only or iRBC egress media treatment in 8-9 individual devices per condition. *(G)* Change in permeability following rAng-1+/-iRBC-egress media treatment normalized by the median value of either the rAng-1+/-media only condition. Box and whisker plots display the median, 25th and 75th percentiles and the minimum and maximum data points in F and G. Statistical significance was analyzed by Mann-Whitney U test.

Discussion:

Disruption of the angiopoietin-Tie axis is a common feature in cerebral malaria patients, often associated with disease severity and fatality (18, 20). This dysregulation is also found in pediatric and adult severe malaria patients without cerebral complications (17, 19) or in placental malaria (50). Central to this pathway are cerebral pericytes, an Ang-1 secreting cell type that is located at the interface between the vasculature and brain parenchyma, yet largely understudied in the context of cerebral malaria. Here, we developed a 3D brain microvessel microfluidic model that recapitulates the high pericyte coverage present in the brain microvasculature. Exposure of the 3D brain microvessels to *P. falciparum*-egress products caused an increase in vascular permeability accompanied by a decrease in Ang-1. Furthermore, we showed that pre-treatment with rAng-1 could, at least, partially protect against endothelial barrier breakdown. Taken together, these results suggest that the cessation of Ang-1 release upon exposure to iRBC-egress products further contributes to microvessel disruption.

The bioengineered 3D model provides important vascular mechanical cues, including estimated flow and extracellular matrix stiffnesses present in the human brain. We could reproduce the high pericyte coverage found in brain capillaries by co-seeding primary cerebral endothelial cells and pericytes through the microfluidic network. Simultaneous cell seeding, at a ratio of 5:1 (endothelial cells: pericytes), did not prevent the formation of an intact luminal endothelial monolayer that presents continuous labeling of adherens and tight junctional markers. SBF-SEM microscopy showed that both cell types sit at nanoscale distance, with the presence of thin lamellae extending from the pericyte soma covering large areas of the endothelium. Yet, despite close proximity, the recently well-described reciprocal peg-and-socket junctions were absent in the model (24). Overall, the 3D brain microvessel model recapitulates pericyte-endothelial interactions found in human brain vasculature making it suitable to study the role of pericytes in CM pathogenesis.

P. falciparum products released during blood stage egress have been shown to possess barrier breakdown capabilities on 2D endothelial monolayers grown on plastic. Proposed barrier disruptive *P. falciparum*-iRBC egress products include merozoite proteins, histones, heme, hemozoin and *P. falciparum* histidine rich protein 2 (22, 44–48, 51). However, their effects on pericytes remain unexplored. In this study, we confirmed that these products are disruptive in a

357 microfluidics-based 3D brain microvessel model in the presence of pericytes. Pericytes play an
358 important role in maintaining vascular homeostasis. For example, loss of pericytes from the
359 cerebral vasculature leads to increased permeability in mouse models (52). Furthermore,
360 dysregulation of cerebral pericytes and detachment from the vasculature have been observed in
361 other cerebral vasculature pathologies including stroke and Alzheimer's disease (26, 27). In our
362 study, we did not observe gross differences on pericyte morphology or loss of vascular coverage
363 upon treatment with iRBC-egress media. Nevertheless, pericytes from iRBC-egress media -
364 treated 3D microvessels did display subtle morphological changes, having significantly less
365 branches. The relevance of these minor ultrastructural modifications in vascular barrier
366 dysfunction could imply molecular mechanisms of disease. For example, Luminex quantification
367 upon stimulation with iRBC-egress media in the 3D brain microvessel model revealed a significant
368 reduction in N-cadherin shedding. This could point towards reduced functional endothelial-
369 pericyte interaction upon short-term incubation with *P. falciparum*-egress products. Future studies
370 should explore whether exposure to *P. falciparum* for longer timepoints recapitulates phenotypes
371 observed in post-mortem samples of cerebral malaria patients such as vacuolization (53) or
372 pericyte loss (29). Nevertheless, our results point towards a loss of integrity at the endothelial and
373 pericyte interface.

374 Ang-1 and Ang-2 have been considered in the past as potential biomarkers of cerebral malaria
375 (54). Ang-1 has excellent predictive power to distinguish malaria severity scores (19) or malaria
376 from other CNS febrile diseases (55). Nevertheless, the underlying mechanism of Ang-1 decrease
377 in CM remains unknown, as previous *in vitro* studies overlooked the effect that iRBCs could exert
378 on brain pericytes. To our knowledge, our study is the first one to report that *P. falciparum*
379 products released upon iRBC egress halt Ang-1 secretion by pericytes. A complementary
380 hypothesis for Ang-1 decrease in CM could be that severe thrombocytopenia, commonly
381 associated with cerebral complications in *P. falciparum* infections (7), could play an additional role
382 as platelets are another major source of serum Ang-1 (56). In light of this, it is likely that both the
383 effect of *P. falciparum*-iRBC on perivascular cells and thrombocytopenia could work in concert to
384 further contribute to a widespread decrease of Ang-1 levels. As for the mechanism of Ang-1
385 secretion cessation, the presence of accumulated light scattering, DAPI-positive iRBC-egress
386 material suggest a role of parasitic DNA or hemozoin, yet further studies are necessary to identify
387 which iRBC-egress derived component is responsible for altered signaling pathways in pericytes.
388 Nevertheless, our results highlight brain pericytes as a new player in the development of CM
389 through dysregulation in the secretion of Ang-1.

The use of recombinant Ang-1 as an adjunctive therapeutic against CM has long been of interest (49) because of its role in strengthening endothelial tight junctions, as well as, upregulating anti-apoptotic and anti-inflammatory pathways (57). Interestingly, we showed that pre-incubation of human microvessels with recombinant Ang-1 partially protected against iRBC-egress mediated barrier breakdown. Nevertheless, the failure to achieve complete protection upon rAng1 supplementation hints at the existence of other pathogenic mechanisms involved in cerebral malaria-induced barrier breakdown. While the concentration of recombinant Ang-1 utilized in this study was supraphysiological compared to peripheral blood samples, it is quite likely that peripheral blood concentrations underestimate local concentrations at the endothelial-pericyte interface. In our model, protection was only achieved after a pre-incubation of 18-hours, suggesting that downstream signaling through the Tie2 receptor, such as PI3K/Akt signaling, is required (10). Future interventions targeting the angiopoietin-Tie axis should focus on approaches that reverse microvascular dysfunction after exposure to *P. falciparum.* As a proof of concept, recombinant Ang-1 has previously been used as a treatment in a rodent experimental cerebral malaria model after onset of disease, preserving blood-brain barrier integrity, and leading to a significantly increased survival rate (49). Although we did not observe protection after short term exposure, our findings point towards a mechanistic role of Ang-1 in protecting against iRBC egress-mediated endothelial barrier breakdown, further highlighting Ang-1 alteration as a functional contributor to CM pathogenesis.

Clinical studies have shown a lack of correlation between Ang-2 levels and iRBC microvascular obstruction in the rectal microvasculature (58) or iRBC sequestration in brain post-mortem samples (59). Similarly, our study confirms that iRBC sequestration in 3D brain microvessel models does not directly cause Ang-2 secretion by endothelial cells. Furthermore, this result is in concordance with a recent study that showed that Ang-2 is not secreted in response to *P. falciparum* lysate products, but rather occurs following endothelial activation with TNF (22). Other studies have shown Ang-2 release as a result of thrombin incubation or hypoxia (23, 60), conditions that have also been associated with CM pathogenesis. Altogether, our study is in agreement with previous reports suggesting that *P. falciparum* sequestration does not play a direct role in the secretion of Ang-2, which instead is more likely a consequence of the activation of host pro-inflammatory factors.

To note, our study has several limitations, including the low-throughput of the model or the impossibility to grow the devices for long periods of time, hence preventing the modelling of long-term disruptive mechanisms, such as pericyte loss. An additional limitation of our model is the

absence of other cells that could play an important role in maintaining the angiopoietin-Tie axis. For example, Ang-1 secretion has been described in other brain and blood cell types, such as smooth muscle cells (61, 62), platelets and more recently, neurons and astrocytes (63). Yet, one of the major advantages of *in vitro* bioengineered models is the opportunity to sequentially introduce different components that, independently or collectively, could play a role in a complex and multifaceted disease such as CM. In light of this, future iterations of the model could introduce other cell types that produce Ang-1 or incorporate pro-inflammatory cytokines or thrombin, to concurrently model the functional consequence of increased secretion of Ang-2 by endothelial cells.

In summary, our study highlights the role that pericytes could have in the development of CM pathogenesis by showing for the first time that egress of *P. falciparum*-iRBC interrupt Ang-1 secretion by pericytes. In addition, our findings confirm that external addition of Ang-1 partially protects against the increase in vascular permeability mediated by *P. falciparum* egress products, suggesting that interventions involving the angiopoietin-Tie axis could be part of a multi-targeted adjunctive therapy against CM.

Materials and Methods:

Parasite lines:

HB3var03 variant *P. falciparum* parasites (dual ICAM-1 and EPCR binding), regularly panned and monitored for appropriate PfEMP1 expression, were cultured in human B+ erythrocytes in RPMI 1640 medium (GIBCO) supplemented with 10% human type AB-positive plasma, 5mM glucose, 0.4 mM hypoxantine, 26.8 mM sodium bicarbonate and 1.5 g/L gentamicin. Parasites were grown in sealed top T75 flasks in a gas mixture of 90% N_2, 5% CO_2 and 1% O_2. To maintain synchronous cultures, parasites were synchronized twice a week in their ring stage with 5% sorbitol and once a week in their trophozoite stage with 40 mg/mL gelaspan (Braun).

P. falciparum-iRBC egress media preparation:

Late-stage *P. falciparum*-iRBC (schizonts, parasitemia of 5-10%), synchronized in a 6-hour window, were purified by use of 40 mg/mL gelaspan gradient separation to a final purity of >60% parasitemia. The enriched *P. falciparum*-iRBC were then placed in complete RPMI media containing 1 µM compound 2, a reversible PKG inhibitor that inhibits iRBC egress (kindly donated by Michael Blackman, The Francis Crick Institute), at a concentration of 50 million *P. falciparum*-

iRBC/mL. After 5 hours, compound 2 containing media was removed and the parasites were resuspended at a concentration of 100 million *P. falciparum*-iRBC/mL in vascular growth media, put into a sealed top T25 flask, gassed and left in the incubator overnight on a shaker set to 50 rpm to facilitate parasite egress. The resulting parasite egress efficiency was assessed by a hemocytometer count and blood smear, and was then concentrated to a working concentration of 50 million ruptured *P. falciparum*-iRBC/mL. The resulting iRBC-egress media is spun at 1000 rpm to remove cellular debris and flash frozen in liquid nitrogen until used. This concentration was chosen as this value is equivalent to a circulating parasitemia of 1%, concentrations frequently found in malaria patients.

Primary human brain microvascular endothelial cell and primary human brain vascular pericyte culture:

Primary HBMEC (Cell Systems; ACBRI 376) were cultured according to the manufacturer's recommendations in complete endothelial growth media-2MV (Lonza) containing 5% fetal bovine serum. Cells were split using Trypsin/EDTA. When 90% confluent, HBMEC were seeded on 15 µg/mL Poly-L-lysine (P8920, Sigma) coated T75 flasks. Primary HBVP (ScienCell) were cultured according to the manufacturer's recommendations in basal pericyte media supplemented with 1% pericyte growth supplement, 1% penicillin/streptomycin and 2% fetal bovine serum (ScienCell). Cells were split using Trypsin/EDTA when 90% confluent, seeded on 15 µg/mL Poly-L-lysine coated T75 flasks, and maintained in a humidified incubator at 37 °C and 5% CO_2. All experiments were conducted with HBMEC and HBVP with a passage number of 7-9.

mCherry lentivirus transduction:

HBVPs were grown in a T75 flask to a ~90% confluency and incubated with lentiviral particles containing a mCherry vector (kindly donated by Kristina Haase Lab, EMBL Barcelona) in serum free pericyte media at a multiplicity of infection of 10. After 24 hours, the lentivirus particles were removed by washing once every 24-hours for a 2-day period. mCherry-positive cells were then selected by fluorescence-activated cell sorting, expanded and froze down for future experiments.

3D brain microvasculature model fabrication:

Type 1 collagen was extracted from rat tails, dissolved in 0.1% acetic acid, lyophilized in a freezer dryer (Labconco Freezone 2.5 Plus) and resuspended at 15 mg/mL in 0.1% acetic acid for storage. The stock collagen solution-0.1% acetic acid solution was neutralized and diluted to 7.5 mg/mL on ice. A 13 by 13 channel grid or single channel pattern were negatively imprinted into

the collagen hydrogel by soft lithography using a PDMS stamp, and inlet and outlets were created by insertion of stainless-steel dowel pins. The top pre-patterned collagen hydrogel contained in a plexiglass top jig is sealed to a flat collagen-layered bottom that sits on a coverslip and a plexiglass bottom jig. The assembly creates perfusable 120 μm diameter microvessels (grid design) or 200 μm diameter microvessels (single channel design), as described previously (33, 64). Prior to cell seeding, the channels were incubated with vascular growth media, consisting in EGM-2MV (Lonza) supplemented with 1x pericyte and 1x astrocyte growth factors (ScienCell) for 1 hour. Primary HBMECs and HBVPs, or mCherry-positive HBVPs (for pericyte coverage analysis), were resuspended at concentrations of 7 million cells/mL and mixed to a ratio of 5:1 HBMECs to HBVPs. The cell mixture was then seeded into the inlet in 8 μL increments and driven through the microfluidic network by gravity-driven flow. Cells were perfused twice from either the inlet or outlet until the channels were completely covered with adhered cells. Media was then removed and devices were flipped upside down for 1-hour to ensure even cell distribution on the top and bottom of the channels. Microvessels were cultured for 3 days before being used in experiments with media change every twice per day by gravity driven flow.

Immunofluorescence microscopy:

Microvessel labeling was performed by gravity driven flow. Microvessels were fixed with 3.7% paraformaldehyde (PFA) in PBS for 15 minutes followed by three 10-minute washes with PBS. Next microvessels were incubated with Background Buster (Innovex) for 30 minutes and then permeabilized with blocking buffer (0.1% Triton X-100 and 2% bovine serum albumin in phosphate-buffered saline (PBS)). Primary antibodies including rabbit anti-αSMA-555 (EPR5368, Abcam), mouse anti-vWF (sc-365712, Santa Cruz), mouse anti-ZO-1 (Invitrogen, 10017242), rabbit anti-β-catenin (Cell Signaling, 9587S), mouse anti-PDGFRβ (Abcam, ab69506), mouse anti-NG-2 (Invitrogen, 10424493), rabbit anti-laminin (Abcam, ab11575), rabbit anti-collagen IV (Abcam, ab6586)), mouse anti-VE-cadherin (sc-52751, Santa Cruz), and Phalloidin-647 (Invitrogen, A22287) were diluted in blocking buffer at 1:100 and incubated overnight at 4 °C. After three 10-minute PBS washes, secondary antibodies including goat anti-mouse Alexa Fluor 488 (A11001, Invitrogen), goat anti-rabbit Alexa Fluor 488 (Invitrogen, A-11008), goat anti-mouse Alexa Fluor 594 (Invitrogen, A-11005), goat anti-rabbit Alexa Fluor 594 (Invitrogen, A-11012), goat anti-mouse Alexa Fluor 647 (A21235, Invitrogen), goat anti-rabbit Alexa Fluor 647 (Invitrogen, A-21244) and 2 mg/mL DAPI (D21490, Invitrogen) were diluted at 1:250 in 2% bovine serum albumin and 5% goat serum containing PBS, and incubated at room temperature for 1 hour. Microvessels were washed 6 times with PBS for 10 minutes each and then imaged on a

Zeiss LSM 980 Airyscan 2. Image stacks were acquired with 3 µm or 10 µm z-step size for single or tile scan images respectively. Z-projections and further threshold analysis was done using Fiji (ImageJ v1.54f) software.

Pericyte coverage analysis:

Tile scan images of the microvessel network with mCherry-positive HBVP and vWF-labeled HBMEC were acquired as described above. Images were divided into two stacks, one being the top half of the microvessels of the network and the other the bottom half. Next, Z-projections of the top and bottom surfaces of the network were generated. The percentage of endothelial surface that was covered by pericytes was calculated by creating a mask of both the mCherry HBVP and the vWF-positive HBMEC.

Serial Block-Face Scanning Electron Microscopy:

Microvessel devices were grown for 3 days, then treated with iRBC-egress media or vascular growth media for 18hours, and then fixed by adding 2% PFA and 2.5% glutaraldehyde (GA) to the device inlet for 30-minutes and washed twice with EGM-2MV at 37 °C. The collagen hydrogel was then carefully removed from the plexiglass jig and microvessel regions exposed to low shear stress were cut out and fixed with a secondary fixative solution (2% PFA, 2.5% GA, 0.25 mM $CaCl_2$, 0.5 mM MgCl, 5% sucrose in a pH 7.4 0.1 M Cacodylate buffer) overnight at 4 °C, and then rinsed twice for 15-minutes with 0.1 M Cacodylate buffer. Samples were post-fixed in a reduced Osmium solution (1% OsO_4, 1.5% K_3FeCN_6 in 0.065 M Cacodylate buffer) for 2-hours at 4 °C followed by six 10-minute washes in dH_2O. Post-staining consisted of subsequent incubation steps of 1% thiocarbohydrazide in dH_2O, 2% Osmium tetroxide in dH_2O, and 1% Uranyl acetate in dH_2O, aided by a PELCO Biowave Pro+ (Ted Pella) containing a SteadyTemp Pro and ColdSpot set to 20 °C at 7x 2 minute cycling on-off at 100 W under vacuum, with dH_2O rinses in between steps once in a fume hood and twice in the microwave at 250 W for 40 s without vacuum. The stained samples were then dehydrated by serial additions of 30, 50, 80, and 100% ethanol solutions in the microwave at 250 W for 40 s without vacuum with ColdSpot set to 4 °C, infiltrated with EPON 812 hard epoxy resin in steps of 25, 50, 75, 90, and 3x 100% resin diluted in ethanol with each step in the microwave at 150 W for 3 minutes under vacuum and polymerized at 60 °C for 48 hours. The sample was trimmed (UC7, Leica Microsystems) using a 90° cryo-trimmer (Diatome) to generate a small block face. The resulting resin block was mounted on a pin stub using silver conductive epoxy resin (Ted Pella). The SBF-SEM acquisition was performed with a Zeiss Gemini2 equipped with a Gatan 3view microtome and a focal charge compensation device

(Zeiss). The SEM was operated at 1.5 kV 300 pA, using a pixel size of 15 nm, a slice thickness of 50 nm and a dwell time of 1.6 µs. The SBF-SEM acquisition was performed using the software SBEMimage (65). The acellular center of the lumen was not imaged to save imaging time. Following acquisition, sections and tiles obtained were aligned and blended using a published method for assembly, stitching and alignment of large EM datasets (66). Aligned images were then binned to 22 by 22 by 250 nm^3 in xyz and segmentation was then performed using the software package Amira (Thermo Fischer Scientific). Primary HBVP and HBMEC were segmented semi manually using the magic wand and brush tool to segment every fifth section followed by use of the interpolation tool to segment the entire volume. The resulting segmented microvessels were rendered using the generate surfaces module for 3D visualization.

P. falciparum-iRBC and iRBC-egress media perfusion:

All experiments were done in 3D microvessel devices grown for 3 days. Schizont-stage *P. falciparum*-iRBC were purified to >60% parasitemia by 40 mg/mL gelaspan and the resulting enriched population was diluted in vascular growth media to 50 million iRBC/mL (same concentration as the *P. falciparum*-iRBC-egress media). 200 µL of *P. falciparum*-iRBC or *P. falciparum*-iRBC-egress media was added into the device inlet and perfused by gravity flow for 30-minutes with the outlet effluent being reintroduced to the inlet every 10 minutes. Microvessels treated with intact *P. falciparum*-iRBC (but not *P. falciparum*-iRBC-egress media), were then washed for 10 minutes with vascular growth media. Both conditions were incubated overnight for 18 hours. Supernatant was then removed from the outlet and pooled for Luminex analysis, and 3D brain microvessels were used for permeability studies or fixed for imaging with 3.7% PFA for 15 minutes (see section immunofluorescence microscopy).

Fluorescent dextran-based permeability assay:

Single channel microvessel devices were grown for 3 days, then perfused and incubated for 18 hours with either vascular growth media or *P. falciparum*-iRBC-egress media as described above. To determine resulting changes in permeability, they were perfused with a 70 kDa FITC-dextran solution as follows: the device was washed 1x with PBS and placed in a Zeiss LSM 980 Airyscan2 confocal microscope with a temperature and CO_2 controlled imaging chamber (37 °C, 5% CO_2). PBS was aspirated and 100 µL of 70 kDa FITC-dextran solution (100 µg/mL) in PBS was pulled from the inlet to the outlet at 6.5 µL/min flow rate using a syringe pump (Harvard Apparatus PHD 2000). Tilescan confocal images of the entire channel were taken every 30 seconds for 5 minutes once the channel had been filled with FITC dextran. In devices pre-treated with recombinant Ang-

1 (923-AB-025, R&D Systems), pre-incubation occurred at 18-hours, starting on day 2. To compare changes in permeability following *P. falciparum*-iRBC-egress media treatment in the presence or absence of rAng-1, the ratio between untreated and treated devices with *P. falciparum*-iRBC was calculated using median values for normalization.

Quantification of apparent permeability:

Apparent permeability is determined as the flux of fluorescently labeled dextran across the microvessel wall into the surrounding collagen hydrogel. All steps of permeability analysis were performed using ImageJ. By using the following equation:

$$Papp = \frac{1}{\mathrm{I_{Vt1}} - \mathrm{I_{Tt1}}} \times \frac{\mathrm{I_{Tt2}} - \mathrm{I_{Tt1}}}{\Delta \mathrm{t}} \times \frac{\mathrm{A_{lateral\ tissue}}}{\mathrm{P}}$$

The apparent permeability (P_{app}) was calculated using the fluorescence intensity inside the vessel (I_V) and in the surrounding collagen hydrogel (I_T) at two time points t1 (0 minutes after the vessel is filled with dextran) and t2 (5 minutes after the vessel is filled). Δt is the change in time, $A_{lateral\ tissue}$ is the area of the collagen hydrogel being examined and P is the perimeter of the microvessel. To account for *P. falciparum*-iRBC-egress material that appears dark even in the presence of 70 kDa FITC-dextran, regions of *P. falciparum*-iRBC-egress material were excluded from the calculation of the fluorescence intensity inside the vessel (I_V) by using ImageJ median smoothing and the magic wand tool to select only the area of the channel without *P. falciparum*-iRBC-egress material.

Serial Block-Face Scanning Electron Microscopy pericyte morphology analysis:

3D-rendered pericyte meshes, segmented from SBF-SEM images of microvessels treated with either media alone or iRBC-egress media, were generated using Amira. Following segmentation, the meshes were exported as *STL* files and processed with a custom-developed Python script, designed to quantify aspects of pericyte morphology, including mesh circularity and maximum width (67). Firstly, the 3D pericyte meshes were mapped onto a 2D plane through principal component analysis (PCA), effectively reducing the data's dimensionality while retaining its most significant morphological features. This mapping uses the two principal components that encapsulate the dimensions with the maximum variance in the 3D mesh, thus ensuring the conservation of structural information. Subsequently, convex hull analysis (68) was applied to delineate the pericyte mesh boundaries, providing a clear representation of each structure's shape by which circularity and maximum width could be measured. The circularity of each mesh is calculated using the convex hull, by assessing the ratio of the area enclosed by the hull to the

square of the hull perimeter, with the formula for circularity given as $4\pi \times Area/Perimeter^2$. This circularity metric provides insight into the roundness of the mesh, where a value closer to 1 indicates a shape that is more circular, and values closer to 0 reflect more elongated or irregular shapes. Additionally, the maximum width is defined by identifying the two farthest points along the convex hull boundary and then calculating the greatest perpendicular distance from this line (connecting the farthest points) to any point within the convex hull. This measurement represents the maximum width of the pericyte mesh by assuming its length is the axis with the greater size. In addition, the number of pericyte branches was calculated manually by counting the number of branches on each 3D rendered pericyte.

Quantification of secreted proteins by Luminex Assay:

Secreted protein concentrations were measured from supernatants taken from the outlets of 3D brain microvessels with a 13 x 13 grid geometry. Supernatants from 2-3 devices exposed to the same condition were pooled, diluted 2X and assayed using a 10-plex Human Luminex Discovery Assay from R&D Systems on a Luminex 100/200. The 10-plex panel included: Ang-1, Ang-2, PDGF-BB, N-cadherin, TIMP-1, ANGPTL4, VEGF, Tie-2, IL-8, and CXCL-1. Protein concentrations were interpolated from a 11-point standard curve of known concentrations of recombinant human proteins provided by the vendor and reported as pg/mL using xPONENT 4.2. 7 out of 10 analytes were in the standard curve quantification range for 100% of measurements recorded, with Timp-1, N-cadherin and IL-8 having 100% of measurements above the upper limit of quantification.

Measuring changes in barrier integrity by xCELLigence:

xCELLigence 96 well PET E-plates (300600910, Agilent) were coated with 15 µg/mL Poly-L-lysine and 5000 HBMECs in 200 µL EGM-2MV were added per well. After cell adherence, the plate was placed into the xCELLigence RTCA SP reader to begin baseline measurement of growth-related changes in cell index (an arbitrary measure of impedance) and the cells were incubated for 3 days until cell index reached a plateau (indicative of cell confluence). Media was changed every two days. For initial testing of the impact of iRBC-egress media on barrier integrity, on the day of the experiment iRBC-egress media was added at concentrations of either 12.5, 25 or 50 million ruptured iRBC/mL. Changes in cell index were measured every 15-seconds for 8 hours and then every 15-minutes for 48-hours. To test the impact of Ang-1 on *P. falciparum*-iRBC-egress media mediated barrier breakdown, iRBC-egress media was added at $50x10^6$ ruptured iRBC/mL after either a 1- or 18-hour pre-incubation with 1 µg/mL of rAng-1. Again, changes in cell index were

measured every 15 seconds for 8 hours and then every 15-minutes for 48-hours. Quantification of partial protection was done by first normalizing each condition to the media only control. Then the area under the curve of the negative values, indicative of barrier breakdown, was calculated using GraphPad Prism (version 10.0.2) where the media only without rAng-1 condition represented an average value of 0 and the iRBC-egress media without rAng-1 condition an average value of 100.

Statistical analysis:

All statistics were obtained by use of GraphPad Prism (version 10.0.2). Non-parametric Mann-Whitney U tests were performed for most experiments, except to calculate Ang-1 protection in the 2D xCELLigence experiment in which a repeated measures one-way ANOVA test with Dunnett's multiple comparisons test was performed. A P-value<0.05 was considered statistically significant.

Author contributions.

R.L and M.B conceived the work. R.L, P.R, R.A, and M.B designed experiments. R.L performed most experiments with assistance of F.K, P.R, H.F, M.M, and R.A. R.L, P.R, H.F, W.M, R.A, Y.S, G.M, M.B analyzed the data. R.L and M.B wrote the original draft of the manuscript. All authors contributed to manuscript writing, revision, editing and suggestions.

Acknowledgements

We want to thank Kristina Haase (EMBL Barcelona) for her support and careful suggestions on the project and manuscript writing, as well as for assistance with the generation of mCherry HBVP with help from Violeta Beltran-Sastre. We acknowledge access to the CRG/UPF flow cytometry facility for mCherry HBVP sorting. We are grateful to Carlota Dobaño (ISGlobal) for access to the Luminex and to Michael Blackman (The Francis Crick Institute) who kindly gifted compound 2. This work was facilitated by the EMBL Electron Microscopy Core Facility (EMCF), with important assistance from Viola Oorschot on sample preparation and processing, and Karel Mocaer and Martin Schorb on image analysis. The great majority of this work was supported by the core program funding of the European Molecular Biology Laboratory (EMBL) and the European Research Council (ERC) under the European Union's Horizon 2020 research and innovation program (Grant agreement no. 948088). F.K is funded through the Marie Skłodowska-Curie grant agreement (101068552). H.F is supported by a fellowship from the EMBL Interdisciplinary (EI4POD) program under Marie Skłodowska-Curie Actions COFUND (847543). G.M. is supported by RYC 2020–029886 I/ AEI/10.13039/501100011033, co funded by European Social Fund

(ESF). ISGlobal received support from the grant CEX2018-000806-S funded by MCIN/AEI/ 10.13039/501100011033, and support from the Generalitat de Catalunya through the CERCA Program. This research is part of the ISGlobal's Program on the Molecular Mechanisms of Malaria which is partially supported by the Fundación Ramón Areces.

Bibliography:

1. A. M. Dondorp, *et al.*, Artesunate versus quinine in the treatment of severe falciparum malaria in African children (AQUAMAT): an open-label, randomised trial. *The Lancet* **376**, 1647–1657, (2010).

2. G. L. Birbeck, *et al.*, Blantyre Malaria Project Epilepsy Study (BMPES) of neurological outcomes in retinopathy-positive paediatric cerebral malaria survivors: a prospective cohort study. *The Lancet Neurology* **9**, 1173–1181, (2010).

3. S. Mohanty, *et al.*, Magnetic Resonance Imaging of Cerebral Malaria Patients Reveals Distinct Pathogenetic Processes in Different Parts of the Brain. *mSphere* **2**, 10.1128/msphere.00193-17, (2017).

4. K. Dorovini-Zis, *et al.*, The Neuropathology of Fatal Cerebral Malaria in Malawian Children. *The American Journal of Pathology* **178**, 2146–2158, (2011).

5. A. Kessler, *et al.*, Linking EPCR-Binding PfEMP1 to Brain Swelling in Pediatric Cerebral Malaria. *Cell Host & Microbe* **22**, 601-614.e5, (2017).

6. J. Storm, *et al.*, Cerebral malaria is associated with differential cytoadherence to brain endothelial cells. *EMBO Molecular Medicine* **11**, e9164, (2019).

7. P. K. Sahu, *et al.*, Determinants of brain swelling in pediatric and adult cerebral malaria. *JCI Insight* **6**, (2022).

8. M. Bernabeu, J. D. Smith, EPCR and Malaria Severity: The Center of a Perfect Storm. *Trends in Parasitology* **33**, 295–308, (2017).

9. S. C. Wassmer, T. F. de Koning-Ward, G. E. R. Grau, S. Pai, Unravelling mysteries at the perivascular space: a new rationale for cerebral malaria pathogenesis. *Trends in Parasitology* **40**, 28–44, (2024).

10. H. G. Augustin, G. Young Koh, G. Thurston, K. Alitalo, Control of vascular morphogenesis and homeostasis through the angiopoietin–Tie system. *Nat Rev Mol Cell Biol* **10**, 165–177, (2009).

11. S. Fukuhara, *et al.*, Differential function of Tie2 at cell–cell contacts and cell–substratum contacts regulated by angiopoietin-1. *Nat Cell Biol* **10**, 513–526, (2008).

12. P. Saharinen, *et al.*, Angiopoietins assemble distinct Tie2 signalling complexes in endothelial cell–cell and cell–matrix contacts. *Nat Cell Biol* **10**, 527–537, (2008).

13. M. R. Siddiqui, C. S. Mayanil, K. S. Kim, T. Tomita, Angiopoietin-1 Regulates Brain Endothelial Permeability through PTPN-2 Mediated Tyrosine Dephosphorylation of Occludin. *PLOS ONE* **10**, e0130857, (2015).

14. P. C. Maisonpierre, *et al.*, Angiopoietin-2, a Natural Antagonist for Tie2 That Disrupts in vivo Angiogenesis. *Science* **277**, 55–60, (1997).

15. S. Gurnik, *et al.*, Angiopoietin-2-induced blood–brain barrier compromise and increased stroke size are rescued by VE-PTP-dependent restoration of Tie2 signaling. *Acta Neuropathol* **131**, 753–773, (2016).

16. J. Golledge, *et al.*, Plasma Angiopoietin-1 Is Lower After Ischemic Stroke and Associated With Major Disability But Not Stroke Incidence. *Stroke* **45**, 1064–1068, (2014).

17. T. W. Yeo, *et al.*, Angiopoietin-2 is associated with decreased endothelial nitric oxide and poor clinical outcome in severe falciparum malaria. *Proceedings of the National Academy of Sciences* **105**, 17097–17102, (2008).

18. F. E. Lovegrove, *et al.*, Serum Angiopoietin-1 and -2 Levels Discriminate Cerebral Malaria from Uncomplicated Malaria and Predict Clinical Outcome in African Children. *PLOS ONE* **4**, e4912, (2009).

19. A. L. Conroy, *et al.*, Whole blood angiopoietin-1 and -2 levels discriminate cerebral and severe (non-cerebral) malaria from uncomplicated malaria. *Malaria Journal* **8**, 295, (2009).

20. A. L. Conroy, *et al.*, Angiopoietin-2 levels are associated with retinopathy and predict mortality in Malawian children with cerebral malaria: A retrospective case–control study*. *Critical Care Medicine* **40**, 952, (2012).

21. V. Jain, *et al.*, Plasma levels of angiopoietin-1 and -2 predict cerebral malaria outcome in Central India. *Malar J* **10**, 383, (2011).

22. C. Gomes, *et al.*, Endothelial transcriptomic analysis identifies biomarkers of severe and cerebral malaria. *JCI Insight* **8**, (2023).

23. U. Fiedler, *et al.*, The Tie-2 ligand Angiopoietin-2 is stored in and rapidly released upon stimulation from endothelial cell Weibel-Palade bodies. *Blood* **103**, 4150–4156, (2004).

24. S. Ornelas, *et al.*, Three-dimensional ultrastructure of the brain pericyte-endothelial interface. *J Cereb Blood Flow Metab* **41**, 2185–2200, (2021).

25. R. Daneman, A. Prat, The Blood–Brain Barrier. *Cold Spring Harb Perspect Biol* **7**, a020412, (2015).

26. F. Fernández-Klett, *et al.*, Early Loss of Pericytes and Perivascular Stromal Cell-Induced Scar Formation after Stroke. *J Cereb Blood Flow Metab* **33**, 428–439, (2013).

27. J. D. Sengillo, *et al.*, Deficiency in Mural Vascular Cells Coincides with Blood–Brain Barrier Disruption in Alzheimer's Disease. *Brain Pathology* **23**, 303–310, (2013).

28. A. P. Sagare, *et al.*, Pericyte loss influences Alzheimer-like neurodegeneration in mice. *Nat Commun* **4**, 2932, (2013).

29. V. Barrera, *et al.*, Neurovascular sequestration in paediatric P. falciparum malaria is visible clinically in the retina. *eLife* **7**, e32208, (2018).

30. K. Haase, M. R. Gillrie, C. Hajal, R. D. Kamm, Pericytes Contribute to Dysfunction in a Human 3D Model of Placental Microvasculature through VEGF-Ang-Tie2 Signaling. *Advanced Science* **6**, 1900878, (2019).

31. M. Bernabeu, *et al.*, Binding Heterogeneity of Plasmodium falciparum to Engineered 3D Brain Microvessels Is Mediated by EPCR and ICAM-1. *mBio* **10**, e00420-19, (2019).

32. C. Howard, F. Joof, R. Hu, J. D. Smith, Y. Zheng, Probing cerebral malaria inflammation in 3D human brain microvessels. *Cell Reports* **42**, 113253, (2023).

33. Y. Zheng, *et al.*, In vitro microvessels for the study of angiogenesis and thrombosis. *Proceedings of the National Academy of Sciences* **109**, 9342–9347, (2012).

34. T. M. Mathiisen, K. P. Lehre, N. C. Danbolt, O. P. Ottersen, The perivascular astroglial sheath provides a complete covering of the brain microvessels: An electron microscopic 3D reconstruction. *Glia* **58**, 1094–1103, (2010).

35. M. T. Uemura, T. Maki, M. Ihara, V. M. Y. Lee, J. Q. Trojanowski, Brain Microvascular Pericytes in Vascular Cognitive Impairment and Dementia. *Front. Aging Neurosci.* **12**, (2020).

36. L. He, *et al.*, Analysis of the brain mural cell transcriptome. *Sci Rep* **6**, 35108, (2016).

37. D. Attwell, A. Mishra, C. N. Hall, F. M. O'Farrell, T. Dalkara, What is a pericyte? *J Cereb Blood Flow Metab* **36**, 451–455, (2016).

38. F. Oliveira, O. Bondareva, J. R. Rodríguez-Aguilera, B. N. Sheikh, Cultured brain pericytes adopt an immature phenotype and require endothelial cells for expression of canonical markers and ECM genes. *Front. Cell. Neurosci.* **17**, (2023).

39. W. Denk, H. Horstmann, Serial Block-Face Scanning Electron Microscopy to Reconstruct Three-Dimensional Tissue Nanostructure. *PLOS Biology* **2**, e329, (2004).

40. C. J. Peddie, *et al.*, Volume electron microscopy. *Nat Rev Methods Primers* **2**, 51, (2022).

41. P. C. Nahirney, P. Reeson, C. E. Brown, Ultrastructural analysis of blood–brain barrier breakdown in the peri-infarct zone in young adult and aged mice. *J Cereb Blood Flow Metab* **36**, 413–425, (2016).

42. L. C. D. Smyth, *et al.*, Markers for human brain pericytes and smooth muscle cells. *Journal of Chemical Neuroanatomy* **92**, 48–60, (2018).

43. R. I. Grant, *et al.*, Organizational hierarchy and structural diversity of microvascular pericytes in adult mouse cortex. *J Cereb Blood Flow Metab* **39**, 411–425, (2019).

44. M. R. Gillrie, *et al.*, Src-family kinase–dependent disruption of endothelial barrier function by Plasmodium falciparum merozoite proteins. *Blood* **110**, 3426–3435, (2007).

45. J. Gallego-Delgado, *et al.*, Angiotensin receptors and β-catenin regulate brain endothelial integrity in malaria. *Journal of Clinical Investigation* **126**, 4016–4029, (2016).

46. P. Pal, *et al.*, Plasmodium falciparum Histidine-Rich Protein II Compromises Brain Endothelial Barriers and May Promote Cerebral Malaria Pathogenesis. *mBio* **7**, 10.1128/mbio.00617-16, (2016).

47. J. Storm, Y. Wu, J. Davies, C. A. Moxon, A. G. Craig, Testing the effect of PAR1 inhibitors on Plasmodium falciparum-induced loss of endothelial cell barrier function. *Wellcome Open Res* **5**, 34, (2020).

48. C. A. Moxon, *et al.*, Parasite histones are toxic to brain endothelium and link blood barrier breakdown and thrombosis in cerebral malaria. *Blood Adv* **4**, 2851–2864, (2020).

49. S. J. Higgins, *et al.*, Dysregulation of angiopoietin-1 plays a mechanistic role in the pathogenesis of cerebral malaria. *Sci Transl Med* **8**, 358ra128, (2016).

50. V. Tran, *et al.*, The Angiopoietin-Tie2 axis contributes to placental vascular disruption and adverse birth outcomes in malaria in pregnancy. *eBioMedicine* **73**, (2021).

51. M. Zuniga, *et al.*, Plasmodium falciparum and TNF-α Differentially Regulate Inflammatory and Barrier Integrity Pathways in Human Brain Endothelial Cells. *mBio* **13**, e01746-22, (2022).

52. A. Armulik, *et al.*, Pericytes regulate the blood–brain barrier. *Nature* **468**, 557–561, (2010).

53. E. Pongponratn, *et al.*, An ultrastructural study of the brain in fatal Plasmodium falciparum malaria. *Am J Trop Med Hyg* **69**, 345–359, (2003).

54. G. M. de Jong, J. J. Slager, A. Verbon, J. J. van Hellemond, P. J. J. van Genderen, Systematic review of the role of angiopoietin-1 and angiopoietin-2 in Plasmodium species infections: biomarkers or therapeutic targets? *Malaria Journal* **15**, 581, (2016).

55. A. L. Conroy, *et al.*, Endothelium-Based Biomarkers Are Associated with Cerebral Malaria in Malawian Children: A Retrospective Case-Control Study. *PLOS ONE* **5**, e15291, (2010).

56. R. L. Nachman, S. Rafii, Platelets, Petechiae, and Preservation of the Vascular Wall. *New England Journal of Medicine* **359**, 1261–1270, (2008).

57. P. Saharinen, L. Eklund, K. Alitalo, Therapeutic targeting of the angiopoietin-TIE pathway. *Nat Rev Drug Discov* **16**, 635–661, (2017).

58. J. Hanson, *et al.*, Microvascular obstruction and endothelial activation are independently associated with the clinical manifestations of severe falciparum malaria in adults: an observational study. *BMC Medicine* **13**, 122, (2015).

59. P. Prapansilp, *et al.*, A clinicopathological correlation of the expression of the angiopoietin-Tie-2 receptor pathway in the brain of adults with Plasmodium falciparum malaria. *Malaria Journal* **12**, 50, (2013).

60. P. Pichiule, J. C. Chavez, J. C. LaManna, Hypoxic Regulation of Angiopoietin-2 Expression in Endothelial Cells*. *Journal of Biological Chemistry* **279**, 12171–12180, (2004).

61. C. Sundberg, M. Kowanetz, L. F. Brown, M. Detmar, H. F. Dvorak, Stable Expression of Angiopoietin-1 and Other Markers by Cultured Pericytes: Phenotypic Similarities to a Subpopulation of Cells in Maturing Vessels During Later Stages of Angiogenesis *In Vivo*. *Laboratory Investigation* **82**, 387–401, (2002).

62. T. Nishishita, P. C. Lin, Angiopoietin 1, PDGF-B, and TGF-β gene regulation in endothelial cell and smooth muscle cell interaction. *Journal of Cellular Biochemistry* **91**, 584–593, (2004).

63. X. Wei, S. Jessa, C. L. Kleinman, T. N. Phoenix, Mapping Angiopoietin1 Expression in the Developing and Adult Brain. *Developmental Neuroscience* **43**, 321–334, (2021).

64. L. Piatti, C. C. Howard, Y. Zheng, M. Bernabeu, "Binding of Plasmodium falciparum-Infected Red Blood Cells to Engineered 3D Microvessels" in *Malaria Immunology*, Methods in Molecular Biology., A. T. R. Jensen, L. Hviid, Eds. (Springer US, 2022), , pp. 557–585.

65. B. Titze, C. Genoud, R. W. Friedrich, SBEMimage: Versatile Acquisition Control Software for Serial Block-Face Electron Microscopy. *Front. Neural Circuits* **12**, (2018).

66. G. Mahalingam, *et al.*, A scalable and modular automated pipeline for stitching of large electron microscopy datasets. *eLife* **11**, e76534, (2022).

67. waleedmirzaPhD, waleedmirzaPhD/cell_analysis_toolkit, (2024), . Deposited February 24, 2024.

68. P. Virtanen, *et al.*, SciPy 1.0: fundamental algorithms for scientific computing in Python. *Nat Methods* **17**, 261–272, (2020).

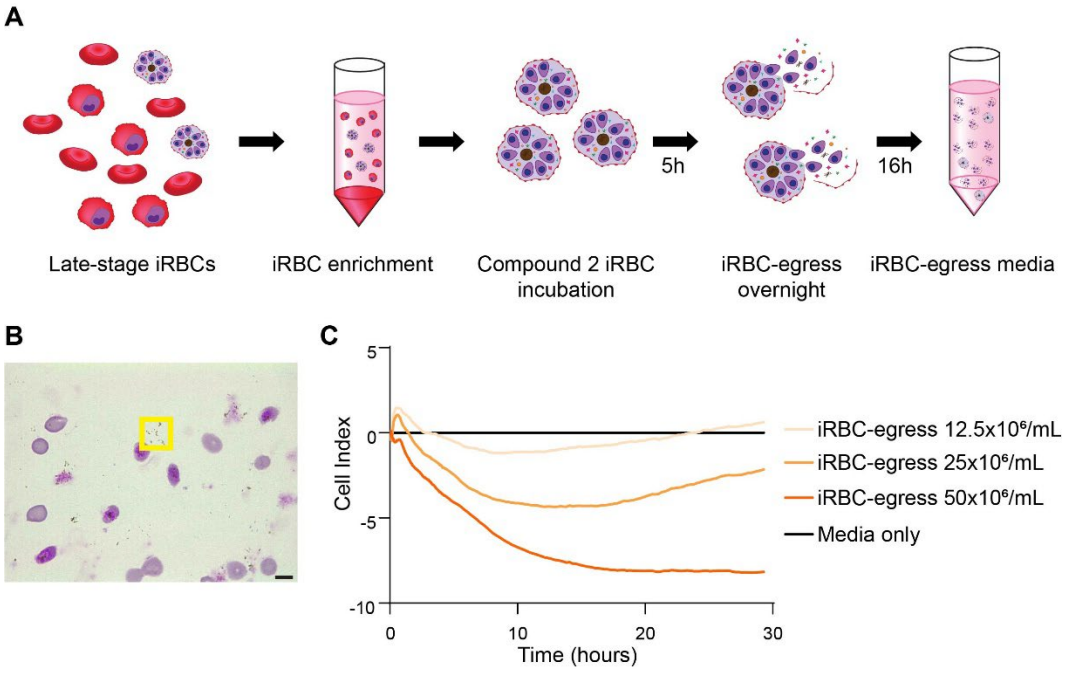

Fig. S1. Preparation of iRBC-egress media that induces barrier breakdown. *(A)* Schematic representation of the protocol to make iRBC-egress media. In short, late-stage *P. falciparum*-iRBC are purified by a gelaspan gradient separation and then incubated for 5 hours with compound-2 to synchronize them at the point of egress. Compound-2 is removed and the *P. falciparum*-iRBC are resuspended in vascular growth media and left overnight on a shaker at 50 rpm to egress. *(B)* A thin smear taken from the resultant iRBC-egress media before centrifugation stained with giemsa. The yellow box highlights free hemozoin particles. Scale bar represents 5 µm. *(C)* Representative recording data of xCELLigence measurements on 2D HBMEC monolayers in the absence of HBVP taken after addition of iRBC-egress media at different concentrations. Data is normalized to the media-only control.

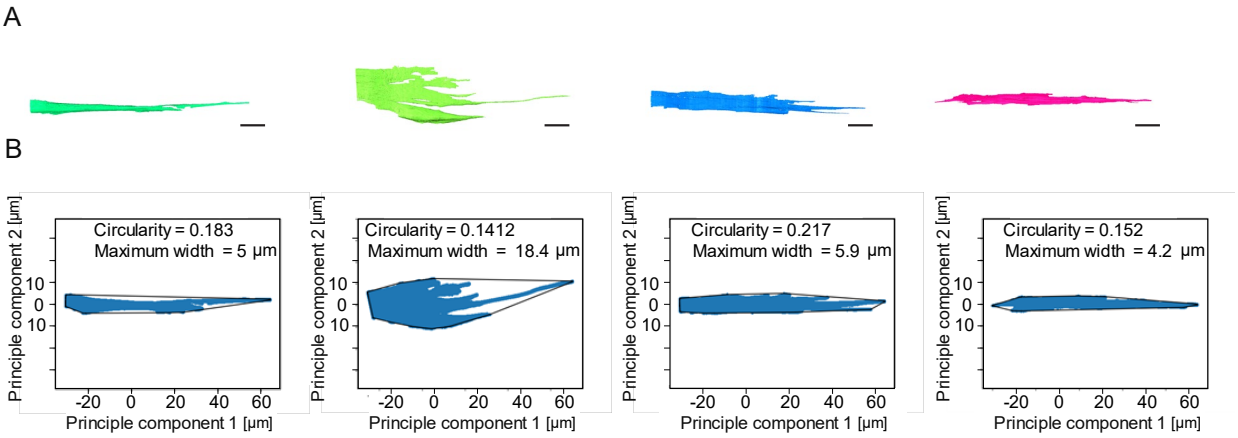

Fig. S2. Morphology analysis of segmented pericytes from SBF-SEM. *(A)* The analysis pipeline begins with the extraction of 3D segmented pericyte meshes. Shown here are four representative pericytes. *(B)* Pericyte geometry is flattened into two principal dimensions using PCA by a Python-based image analysis pipeline. The 2D geometry's shape is then determined using convex hull analysis. To describe pericyte morphology, pericyte cell borders are analyzed for circularity, calculated as 4π*Area/Perimeter^2, where a value of 1 indicates a perfect circle and values approaching 0 indicate increasingly elongated shapes, and maximum width.

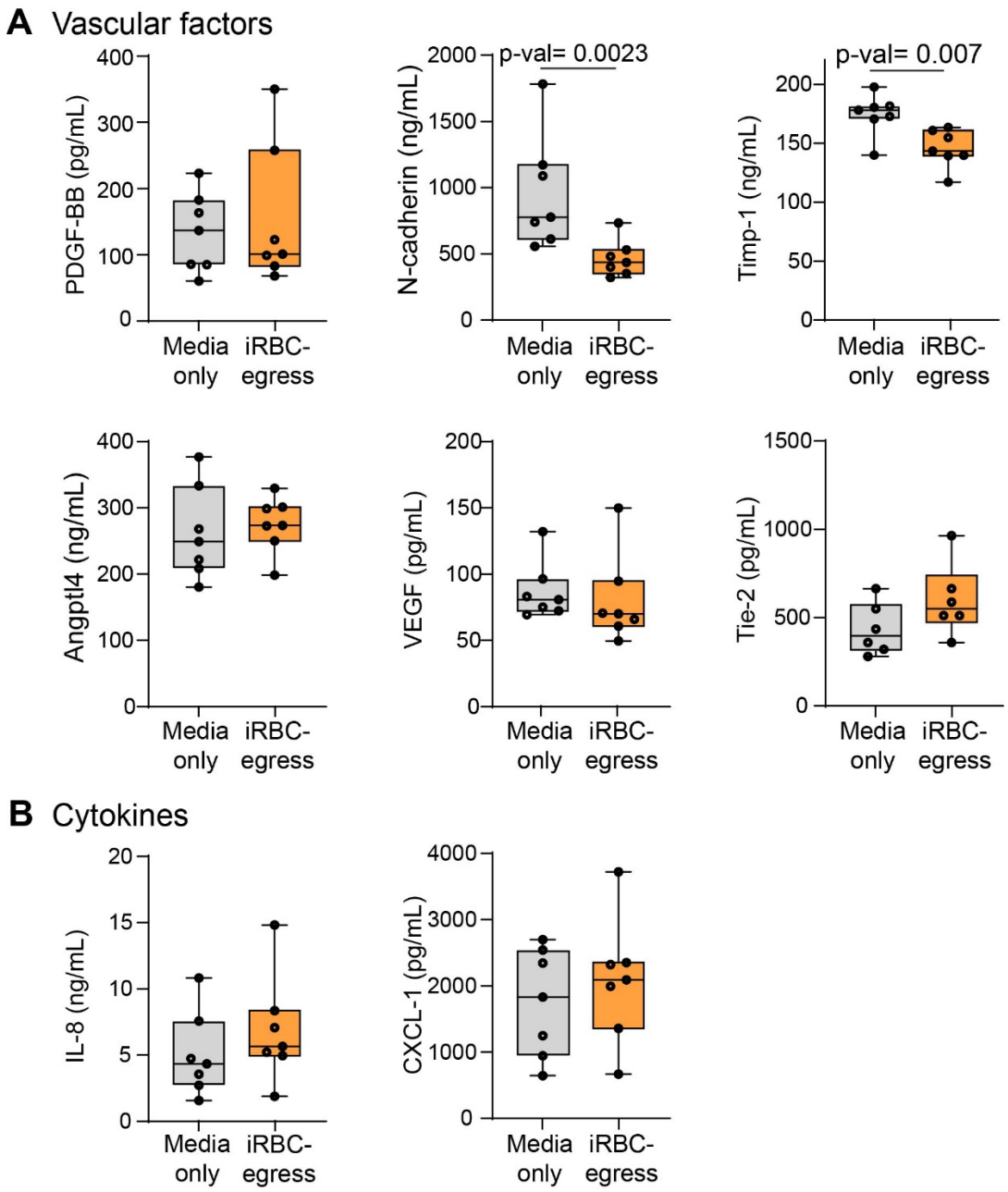

Fig. S3. Changes in secreted vascular factors and cytokines following iRBC-egress media incubation. *(A)* Concentrations of vascular factors PDGF-BB, N-cadherin, Timp-1, Angptl4, VEGF and Tie-2 measured by Luminex from 3D brain microvessels supernatants treated with media only or iRBC-egress media for 18-hours. *(B)* Concentrations of released cytokines IL-8 and CXCL-1 measured by Luminex from 3D brain microvessels supernatants treated with media only or iRBC-egress media for 18-hours. Box and whisker plots display the median, 25th and 75th percentiles and the minimum and maximum data points in A and B. Data points represent supernatants pooled from 2-3 devices in 6-7 independent experiments. Statistical significance is analyzed by Mann-Whitney U test.

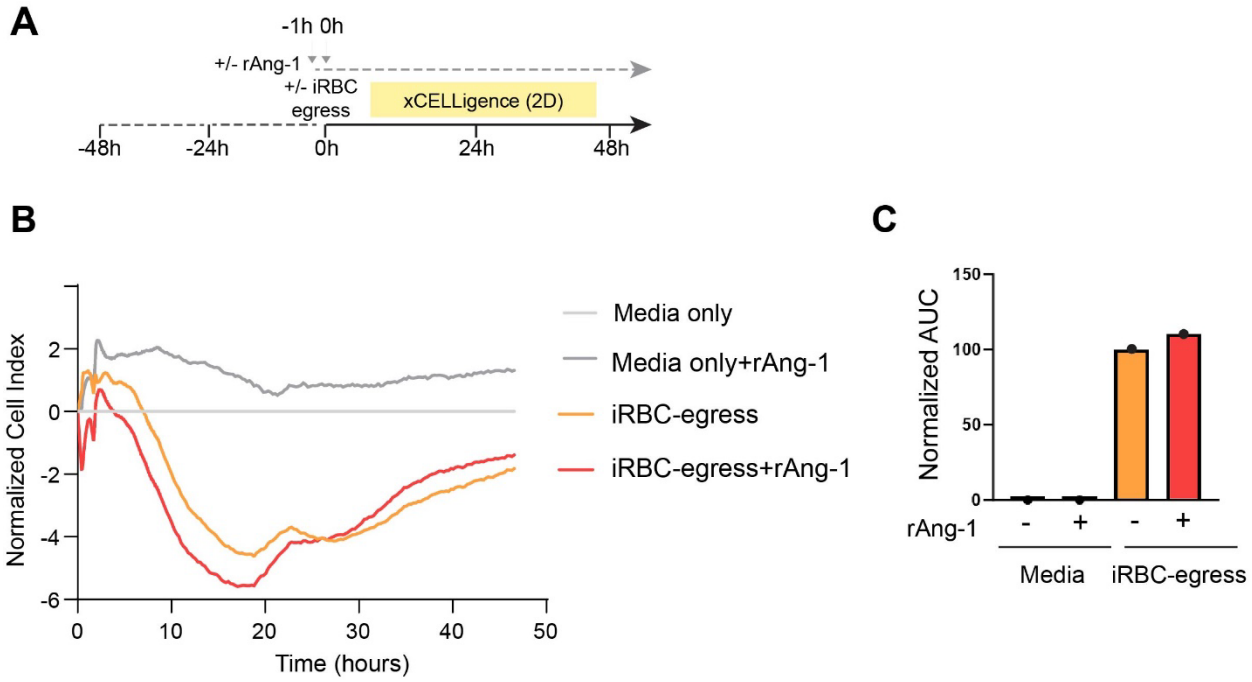

876

877 **Fig. S4.** Short time pre-incubations with rAng-1 does not protect against increased permeability
878 induced by iRBC-egress media. (A) Experimental outline of short-term (1-hour) incubation with
879 rAng-1 in a 2DHBMEC monolayer in the absence of HBVP. (B) Representative recording data of
880 xCELLigence measurements taken after +/- addition of rAng-1. All conditions were normalized to
881 the media only control. (C) Area under the curve analysis. All conditions were normalized to *P.*
882 *falciparum*-iRBC-egress media as 100. Data points represent 1 independent experiment run in
883 triplicate.

884